Natural Resources Canada | Ressources naturelles Canada

GEOLOGICAL SURVEY OF CANADA
OPEN FILE 8890

Using shallow temperature measurements to evaluate thermal flux anomalies in the southern Mount Meager volcanic area, British Columbia, Canada

X. Liu, Z. Chen, and S.E. Grasby

2022

Canada

GEOLOGICAL SURVEY OF CANADA
OPEN FILE 8890

Using shallow temperature measurements to evaluate thermal flux anomalies in the southern Mount Meager volcanic area, British Columbia, Canada

X. Liu, Z. Chen, and S.E. Grasby

2022

Permanent link: https://doi.org/10.4095/330009

This publication is available for free download through GEOSCAN (https://geoscan.nrcan.gc.ca/).

Recommended citation

Liu, X., Chen, Z., and Grasby, S.E., 2022. Using shallow temperature measurements to evaluate thermal flux anomalies in the southern Mount Meager volcanic area, British Columbia, Canada; Geological Survey of Canada, Open File 8890, 19 p. https://doi.org/10.4095/330009

Publications in this series have not been edited; they are released as submitted by the author.

Table of Contents

Abstract

Geothermal is a clean and renewable energy resource. However, locating where elevated thermal gradient anomalies exist is a significant challenge when trying to assess potential resource volumes during early exploration of a prospective geothermal area. In this study, we deployed 22 temperature probes in the shallow subsurface along the south flank of the Mount Meager volcanic complex, to measure the transient temperature variation from September 2020 to August 2021. In our data analysis, a novel approach was developed to estimate the near-surface thermal distribution, and a workflow and code with python language have been completed for the thermal data pre-processing and analysis. The long-term temperature variation at different depths can be estimated by modelling, so that the relative difference of deducing deeper geothermal gradient anomalies can be assessed. Our proposed inversion and simulation methods were applied to calculating the temperature variation at 2.0 meters depth. The results identified a preferred high thermal flux anomalous zone in the south Mount Meager area. By combining with previous studies, the direct analysis and estimation of anomalous thermal fields based on the collected temperature data can provide a significant reference for interpretation of the regional thermal gradient variation.

1. Introduction

Thermal gradient surveys can aid evaluation of a thermal resource volume, identifying possible fracture zones that conduct hydrothermal fluids, and development planning. Sestini (1970) explained in inhomogeneous terrain that heat flow data alone can provide accurate information regarding productive zones. Rybach (1989) presented a heat flow study as a significant parameter for understanding the thermal conditions and processes at depth. Erkan et al. (2005) analysed temperature-depth data from numerous deep wells to characterize the thermal regime. Some algorithms have been presented (e.g. Bennett, 2008), for estimating surface heat flux, in which a summary of the heat flow techniques commonly used in geothermal exploration was given.

Near surface heat flux is an important element for analysis of vertical thermal distributions and the related numerical calculating methodology has been developed for decades. In shallow soil studies, Gao et al. (2010, 2017) compared different methods for thermal flux evaluation, and used a novel approach to evaluate soil heat flux (SHF), and compared previous methods for calculation, including the calorimetric method and methods based on analytical solutions of the heat diffusion equation. Although the temperature of rock or soil at the shallow earth surface is mainly influenced by solar heating, the collected

underground temperature variation still includes some thermal information from the upwards heat flux from deep earth sources. Assouline et al. (2019) presented a Fourier modelling strategy to estimate the apparent thermal diffusivity, and applied this to several locations in Switzerland. Sharratt (1992) presented a finite difference method to calculate the thermal conductivity with a transient heat flow equation, and the comparison shows that the finite difference is better than the harmonic method.

While those methods can determine the thermal flux, uncertainties in soil thermal properties and environmental variation make the calculated results biased. For example, the land cover condition is in part a function of varying physical conditions, influencing estimation of soil/rock thermal properties that is a prerequisite for quantifying temperature changes in time. Thermal conductivity and thermal diffusivity need to be added for modelling analysis, in particular for combined models for heterogeneous lithology, which vary along with the temperature and have seasonal change. This means that the calculated thermal conductivity without considering those factors may not represent its true nature, as such the thermal flux prediction might not be reasonable.

Near-surface temperature monitoring can help to identify higher thermal anomaly that might be related to permeable fracture zones, which will increase score of geothermal resource evaluation, furthermore for supporting reaching net-zero emissions. In order to reduce the effect of thermal properties to upward thermal flux, to estimate the zones of anomalous heat flux, this study is focused on determining the near surface anomalies of temperature and thermal flux at different depths. Since daily and seasonal temperature variation at near surface contains information from upward geothermal flux, the observed thermal variation can be converted into quantitative estimates of flow parameters. We propose a method to estimate the near-surface thermal distribution with a thermal inversion workflow, then simulate the thermal variation in time series, which is used to predict the temperature at deeper location. The calculated distributions are analyzed using statistical methods for locating possible thermal anomalies. The performance of the method is validated in determining soil heat flux, and the results are compared with previous studies. Our results will provide useful reference for heat transfer simulation and resource assessment, and the calculated flow distribution will benefit future exploration, and design of drilling plans.

2. Previous work

The Mount Meager is located approximately 170 km north of Vancouver in undeveloped mountainous country (Fig. 1(a)). It lies at the northern end of the Garibaldi Volcanic Belt, which is the northern Canadian,

extension of the volcanic Cascade Range in the United States. Access has been limited since the landslide of 2010 (Guthrie et al., 2012) washed out the bridge over the Lillooet River, although a new logging road has provided limited access since 2021. The initial surface geologic mapping and radiometric age dating of volcanic and intrusive rocks in the Mount Meager area was done by Read (1979). Additional geological work and resulting information was briefly summarized by B.C. Hydro (1983). The Mount Meager volcanic complex is a geologically young volcano that was active from about 2 Ma to a few thousand years ago (pink contour in Fig. 1(b)), and still expresses thermal springs and fumaroles today (Read, 1979; GeothermEx, 2004). The volcanic sequences consist of andesitic lava flows and pyroclastic units, and dacite and rhyodacite domes and flows, and the basement beneath the volcanic complex comprises intrusive quartz diorite and granodiorite and metamorphic rocks. The wells drilled at the South Meager prospect on the southern flank of the massif penetrate into older intrusives, along with lesser dikes and hydrothermal breccias (GeothermEx, 1995). The breccias are typical of active and fossil geothermal systems, and the close association between the dikes and the breccias suggests significant heating and subsequent fracturing of the host rock. Such fracturing is an *a priori* necessity for development of the hydrothermal system, because it creates the permeability in crystalline rocks that is needed to allow hot water to convect from deeper, hotter levels (as in the vicinity of cooling magma) into the shallower environments that can be reached by drilling (GeothermEx, 2004).

The Mount Meager geothermal area has been explored for almost 50 years. In response to the Energy Crises in 1970s, Canada initiated a Geothermal Energy Program and provided the first insight of the thermal regime of Canada (Fairbank et al., 1983; Jessop, 2008). This work listed some of the highest temperature geothermal systems in Canada which is related to volcanic belts in British Columbia and Yukon. During previous study (before 2010), some geothermal-exploration wells were drilled in south Mount Meager which showed high temperature geothermal resources (>250^{o}C) and high thermal gradients. In recent years, with the rising interest in geothermal potential in Canada, some new research projects have been done in this area (Grasby et al., 2012, 2020), which includes integrated interpretation with geological lineament, geophysical seismic & MT, and rock samples analysis etc. datasets for geothermal resource assessment. Such evaluation better defines the subsurface resource, reducing the drilling cost and exploration investment risk.

Although integrated methods have been applied for supporting this thermal resource evaluation, additional research is required to identify the thermal flux path and permeable zone accurately, including

regional and local hydrologic effects on temperature. This is the main incentive for which temperature probes were deployed in this area, and related data processing and analysis was developed in this study.

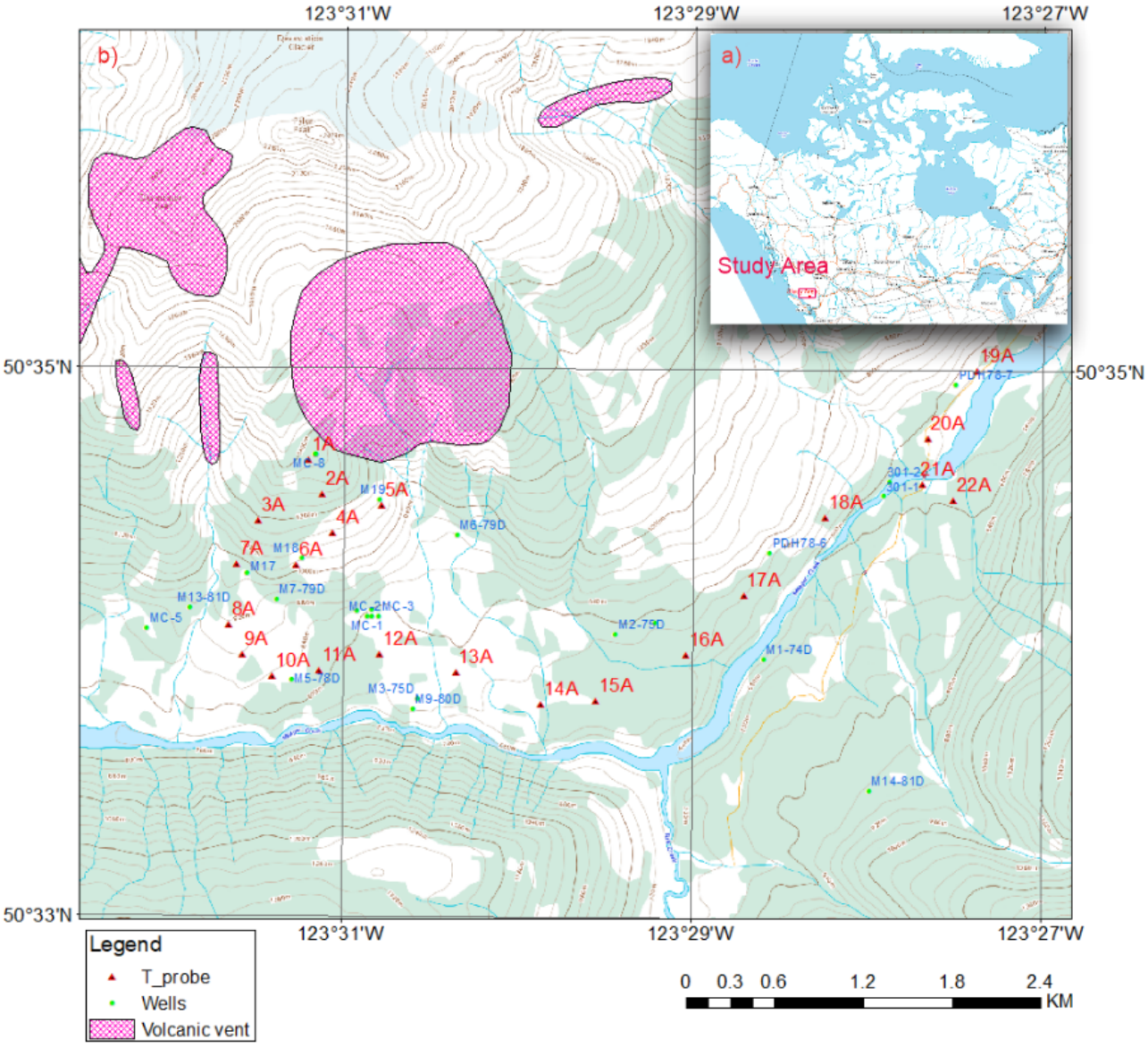

Figure 1. (a) Location of study area; (b) Station distribution of temperature probes (red triangle) in south Mount Meager, (source of base map: http://wms.ess-ws.nrcan.gc.ca/wms).

3. Methodology

3.1 Modeling methods for heat flux

In micrometeorology, measurement of soil heat flux is often considered within the context of the surface energy balance closure,

$$R_n - G = LE + H, \tag{1}$$

where R_n is the net radiation; G is the soil heat flux density at the soil surface; LE is latent heat flux; H is sensible heat flux (Sauer, 2007; Gao, 2010).

The temperature at any point changes at a rate proportional to the local gradient in the heat flow, as the conservation of energy equation:

$$\rho c \frac{\partial T}{\partial t} = -\nabla \cdot J \tag{2}$$

For a one-dimensional model, the conservation of energy equation (1) can be written in the general form:

$$\rho c \frac{\partial T}{\partial t} = -\frac{\partial T}{\partial z}(\lambda \frac{\partial T}{\partial z}), \tag{3}$$

where the J is energy flux; the T is temperature; λ is thermal conductivity; c is the soil specific heat capacity; ρ is soil bulk density; z is vertical distance; $c_v = \rho c$; $\kappa = \frac{\lambda}{c_v}$ is the thermal diffusivity (ms^{-2}).

In a discrete form of equation (3), based on the finite difference form of the transient heat flow equation, the equation for a soil with three nodes (two layers) can be written as (Campbell, 1985),

$$\lambda_2 \frac{\Delta T_2}{\Delta z_2} - \lambda_1 \frac{\Delta T_1}{\Delta z_1} = c(T_2^{j+1} - T_2^{j}) \frac{\Delta z_3}{\Delta t}, \tag{4}$$

where $\Delta T_2 = T_3 - T_2 = (T_3^{j+1} + T_3^{j})/2 - (T_2^{j+1} + T_2^{j})/2$, is the temperature difference, and $\Delta T_1 = T_2 - T_1 = (T_2^{j+1} + T_2^{j})/2 - (T_1^{j+1} + T_1^{j})/2$; $\Delta z_1 = z_2 - z_1$, $\Delta z_2 = z_3 - z_2$, and $\Delta z_3 = (z_3 - z_1)/2$ are the depth interval. The analytical solutions of equation (4) are available for a variety of heat sources, flow geometries, and for different boundary conditions.

Another approach for modeling the heat flow is using a harmonic analysis of soil temperature at one depth. Based on the harmonic analysis, the solution of soil temperature can be described simply using the following function, (Horton, 1983; Hurley, 1993; Sauer, 2007; Assouline, 2019).

$$T(t,z) = T_{0,z} + \sum_{n=1}^{M}\{A_n \exp\left(-\frac{z\cdot\sqrt{n}}{d}\right) \sin(n\omega t + C_n - \frac{z\cdot\sqrt{n}}{d}))\}, \tag{5}$$

where M is the number of harmonics; $T_{0,z}$ is the initial temperature, and T is the diurnal amplitude of surface temperature; A_n and C_n are the n^{th} amplitude and phase of the harmonics. In this study, we assume the phase difference is a function of thermal diffusivity, where $d(\kappa) = \sqrt{\frac{2\kappa}{\omega}}$, is the damping depth, ω is angular frequency and κ is apparent thermal diffusivity.

Figure 2 shows the simulated temperature variation over 48 hours under ideal conditions, where the thermal conductivity is 0.9 $Wm^{-1}K^{-1}$ and the thermal diffusivity is $6 \times 10^{-7} m^2 s^{-1}$ (Gao et al., 2017). The temperature profile shows heat transport under steady-state flow of heat through media at different depths, which indicates the daily solar thermal effect will be negligible at deeper zones (>1.0 m). Since an assumed near surface geothermal thermal anomaly will affect the downward penetration of solar radiation, this assumed model for calculating the temperature can be useful to estimate the subsurface thermal flux by combining seasonal analysis.

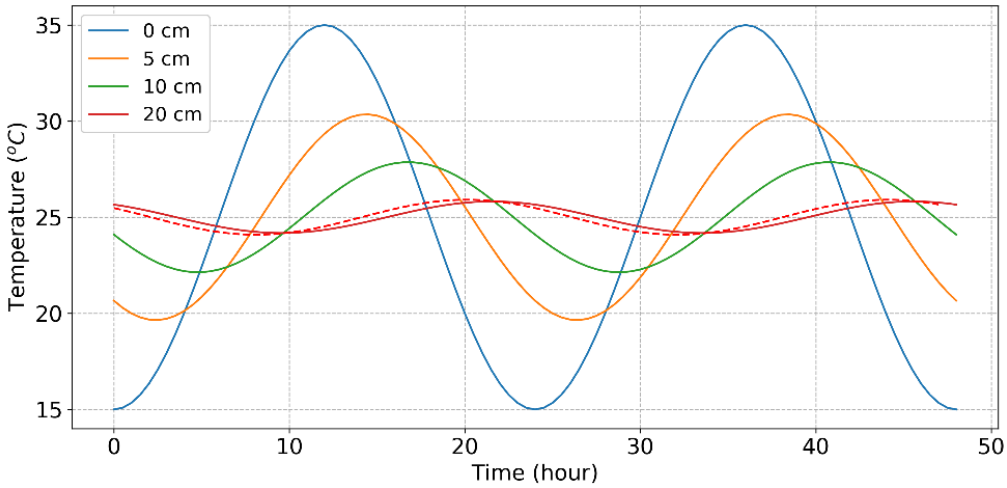

Figure 2. The simulated temperature variation for different depths due to the daily solar effect in ideal condition.

3.2 Inversion workflow

One simple method to calculate A_n and C_n in eq. (5) is using the Fast Fourier Transform (Sauer et al., 2007; Assouline, 2019). In order to be able to use specific frequency range, e.g. daily and annual period, and increase the flexibility of solution of the harmonic equation (eq. (5)) to estimate temperature at depth, we assumed the underground apparent thermal diffusivity of rock/soil is constant in this area, and employed classic inversion algorithm to calculate the variables. Based on the previous modeling methods for calculating subsurface heat flux, we created an objective function of temperature variation and employed a geophysical inversion workflow to solve the misfit function. Both daily and annual frequencies are used in the function. Then the calculated amplitude and phase can be applied for simulation. We assume the discrete inverse problem $d = A(m)$ is a continuous operator from a model space M to a data space D. For any $d \in D$ and any parameter $\alpha \geq 0$, there is a model $m_\alpha \in M$, on which the functional:

$$P^\alpha(m) = \sum_{i=1}^{n}(A_i(m) - d_i)^2 + \alpha \sum_{j=1}^{m}(m_j - m_{apr})^2 = min, \quad (6)$$

where eq. (6) is composed of the misfit function and stabilizing functional. We used a gradient-type technique, the regularized conjugate gradient (RCG) method (Zhdanov, 2002) to calculate the unknown parameters, as shown in the following steps:

$$R_n = A(m) - d \tag{7}$$

$$l_n^{\alpha n} = l^{\alpha n}(m_n) = F_n^* W_d^2 R_n + \alpha W_m^2 (m - m_{apr})$$

$$\beta_n^{\alpha n} = \|l_n^{\alpha n}\|^2 / \left\|l_{n-1}^{\alpha n-1}\right\|^2$$

$$\tilde{l}_n^{\alpha n} = l_n^{\alpha n} + \beta_n^{\alpha n} \tilde{l}_{n-1}^{\alpha n-1}$$

$$\tilde{l}_0^{\alpha 0} = l_0^{\alpha 0}$$

$$k_n^{\alpha n} = (\tilde{l}_n^{\alpha n T} l_n^{\alpha n}) / \{\left\|W_d F_n^* \tilde{l}_n^{\alpha n}\right\|^2 + \alpha \left\|W_m \tilde{l}_n^{\alpha n}\right\|^2\}$$

$$m_{n+1} = m_n - k_n^{\alpha n} \cdot \tilde{l}_n^{\alpha n T},$$

where $A(m)$ is the general analytical solution of harmonic analysis; R_n is the residual in data space; $l_n^{\alpha n}$ is the gradient direction; F_n^* is the adjoin operator of the Frechet derivative matrix; m_{apr} is the reference model; $k_n^{\alpha n}$ is the step length, d is the measured time series temperature; m is the unknown modeling parameter. W_d is the data weighting, and W_m is the model weighting. Here α is the regularization parameter at the n^{th} iteration that provides a balance between the misfit and stabilizing functional. The initial value of the regularization parameter α_o is determined with:

$$\alpha_o = \frac{W_d^2 \|F(m) - d\|^2}{W_m^2 \|m - m_{apr}\|^2} \tag{8}$$

In order to use the RCG method for the minimization of the parametric function, it is necessary to calculate the first derivative of the data parameters with respect to the model parameters, e.g. Fréchet derivatives:

$$F_m = \{\frac{\partial P(m_1)}{\partial m_1} \cdots \frac{\partial P(m_i)}{\partial m_i} \cdots \frac{\partial P(m_M)}{\partial m_M}\}, \tag{9}$$

F_m is the calculated derivative. Figure 3 shows the schematic procedure of RCG inversion. Based on this workflow, we developed python code for thermal flux modelling and inversion procedure, which can calculate the temperature at different depths.

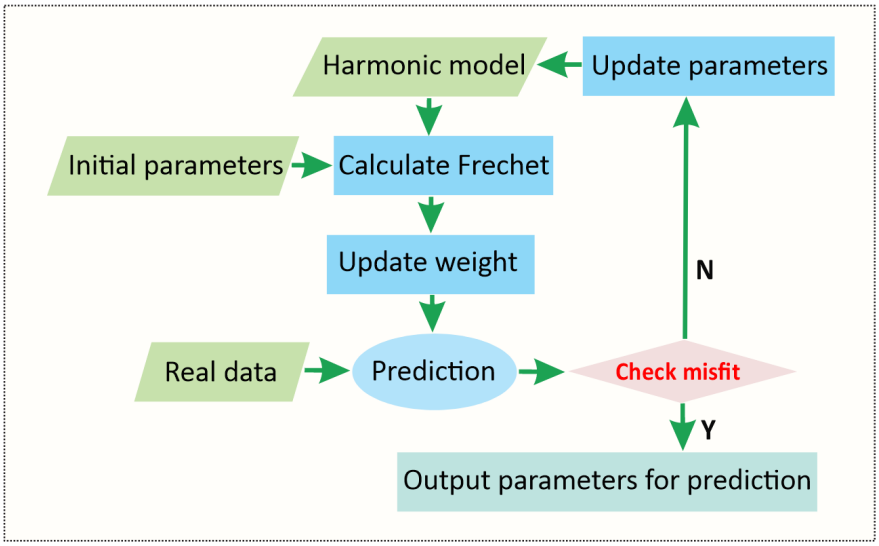

Figure 3. Workflow of RCG iteration for predicting model parameters.

After obtaining the parameters of model, the daily estimates of temperature can be calculated with equation (5). Equation (10) is expressed in an equivalent form to calculate the heat flux density for each time interval i, then the heat flow at depth can be calculated with Fourier's first law (Fourier, 1822; Sauer, 2007):

$$G_i = -k_i \frac{\Delta T_i}{\Delta z_i},\ i = 1, 2 \cdots \tag{10}$$

Figure 4 shows a modelling annual temperature distribution and its simulation with the inversed harmonic functions. The raw data was downloaded from the weather database (red dashed line). The same physical parameters from Figure 2 were used. We can see the trend of temperature variation with increasing depth (0.5, 1.0, 2.0 meter). Based on the model testing results, the proposed method can be used for real data processing and simulating the downward temperature distribution and its annual variation characterization.

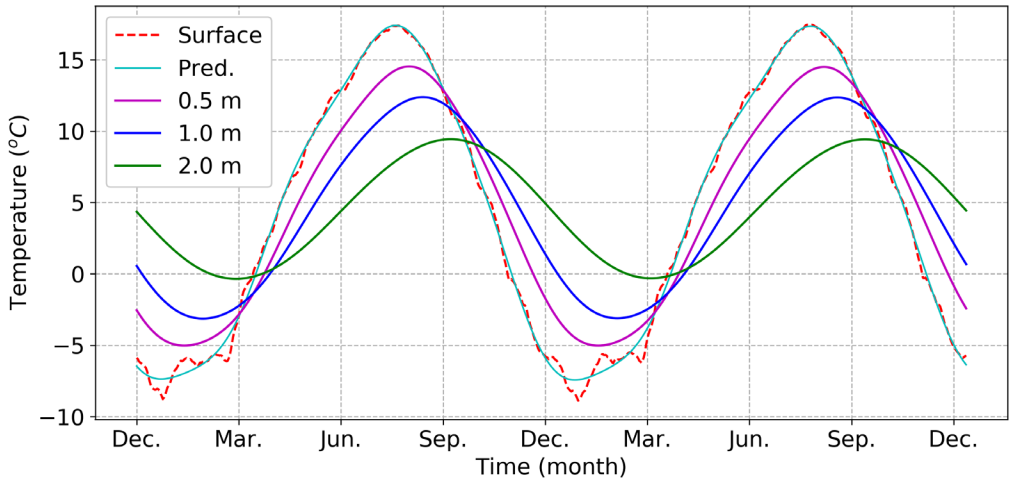

Figure 4. Plots of the inversion testing results and simulated downward annual thermal (daily average) variation (2019-2021).

4. Real data collection, analysis, and evaluation

Under the ongoing GNES program, the Garibaldi Volcanic Belt study is examining new methods to help reduce exploration risk for blind geothermal resources. Besides geologic, geophysical, and geochemical studies, temperature probes were deployed in the Mount Meager volcanic area (Grasby et al., 2020). The datasets used for this study were collected from the southern Mount Meager area. We use these real data to test our methods. The temperature records and thermal flux anomaly are as discussed below.

4.1 Thermal properties and probe

The thermal properties reflect the amount of heat transferred through a unit area in unit time (heat flux density) under a unit temperature gradient. The soil thermal conductivity (λ) is dependent primarily upon the bulk density of the soil and its water content. Following an empirical relationship proposed in Lu et al. (2014), λ is considered as the apparent thermal conductivity, as latent heat transfer in the form of water vapor, and cannot be separated from the heat conducting transport form (Selker, 2019; Hiraiwa and Kasubuchi, 2000). The best fit relationship between λ ($Wm^{-1}K^{-1}$) and θ, power relationships between soil volumetric water content (θ) and the corresponding parameters can be described as:

$$\lambda = 0.2 + \exp(1.46 - \theta^{-0.34}), \tag{11}$$

where 0.20 $Wm^{-1}K^{-1}$ is the thermal conductivity of dry soil and 1.46 and 0.34 are shape factors of the fit curve, which are fitted using a global optimization algorithm (Vrugt et al., 2003; Gupta, 2007; Fuchs, 2015).

Soil water improves the thermal contact between the soil particles, and replaces air, which has 20 times lower thermal conductivity than water. In this study, we tested two sets of apparent thermal conductivity and thermal capacity values for summer and winter periods. Table 1 lists some thermal properties as reference.

Table 1. Thermal properties of soil constituents (Hillel, 1980; Brutsaert, 1982).

Constituent	**λ** $[Wm^{-1}K^{-1}]$ at 10℃	Specific heat capacity $[Jkg^{-1}K^{-1}]$	Density $[kgm^{-3}]$	Volumetric heat capacity $[MJm^{-3}K^{-1}]$
Quarts	8.8	741	2650	2.1
Soil minerals (avg.)	2.9	733	2650	1.94
Soil organic matter	0.25	1926	1300	2.5
Water (liquid)	0.57	4182	1000	4.18
Ice (at 0℃)	2.2	2108	919	1.938
Air	0.025	1005	1.2	0.0012

The probe used in this study are Hobo Water Temp Pro v2 made by Onset. The logger's recordable temperature range is from -40 °C to 70 °C with ±0.2 °C accuracy and 0.02 °C resolution, which records at half hour interval and holds a battery that can support about six years of data logging. The geographic location of temperature probes is shown with red triangles in Figure 1(b).

Table 2. The shadiness index and burial depth of all sites

Site ID	1A	2A	3A	4A	5A	6A	7A	8A	9A	10A	11A	12A	13A	14A	15A	16A	17A	18A	19A	20A	21A	22A
Shadiness index	0.2	0.05	0.1	0.7	0.1	0.4	0.5	0.3	0.5	0.6	0.8	0.6	0.5	0.6	0.8	0.7	0.6	0.8	0.6	0.4	0.9	0.95
Burial depth (cm)	2	1	2	5	4	5	4	2	5	3	3	3	6	2	4	3	6	4	2	3	7	4

4.2 Data analysis and interpretation

The data were collected from September 2020 to August 2021. The burial depth of probes is displayed in Table 2. When the surface was covered with low thermal conductivity snow, this blocked the solar heat flux so that the distribution of temperature is stable without daily variation. In order to analyse the data at the same scale, we selected temperature datasets with the same time periods in summer or winter. In Figure 5 and 6, showing the plots of selected sample sites and periods, we can see the temperatures record the daily variation of solar thermal flux and simulated temperature variation. The calculated temperature at different depths are plotted to display the decreasing effects of solar radiance with increasing depth. The temperature at 1.0 and 2.0 meters depth displays the least daily sunlight affect (purple and brown dashed line). We assumed that the apparent thermal flux from below is a constant. The predicted variation in the thermal gradients related to upwards heat flux are used for statistic analysis. Also we can see those sites exposed under sunlight, the temperature variation become stable as depth increases (site 1A in Fig. 5 and Fig. 6). The statistics results of temperature at 2.0 m during winter is plotted in Figure 7, which identifies some anomalous spots, e.g. 15A, 16A, 21A.

For easier interpretation of predicted temperature at depth, the statistical results of four component indexes are calculated. According to the energy balance equation (eq. (1)), the temperature gradient will be affected by subsurface thermal flux. This means the shape of temperature variation includes the upward thermal information, so the thermal variation gradient and its relative anomalous index are calculated for interpretation. The four component indexes are gradient components in positive and negative directions; temperature difference at 2.0 meters depth; and average temperature during winter. We assume that thermal conductivity is constant for all sites.

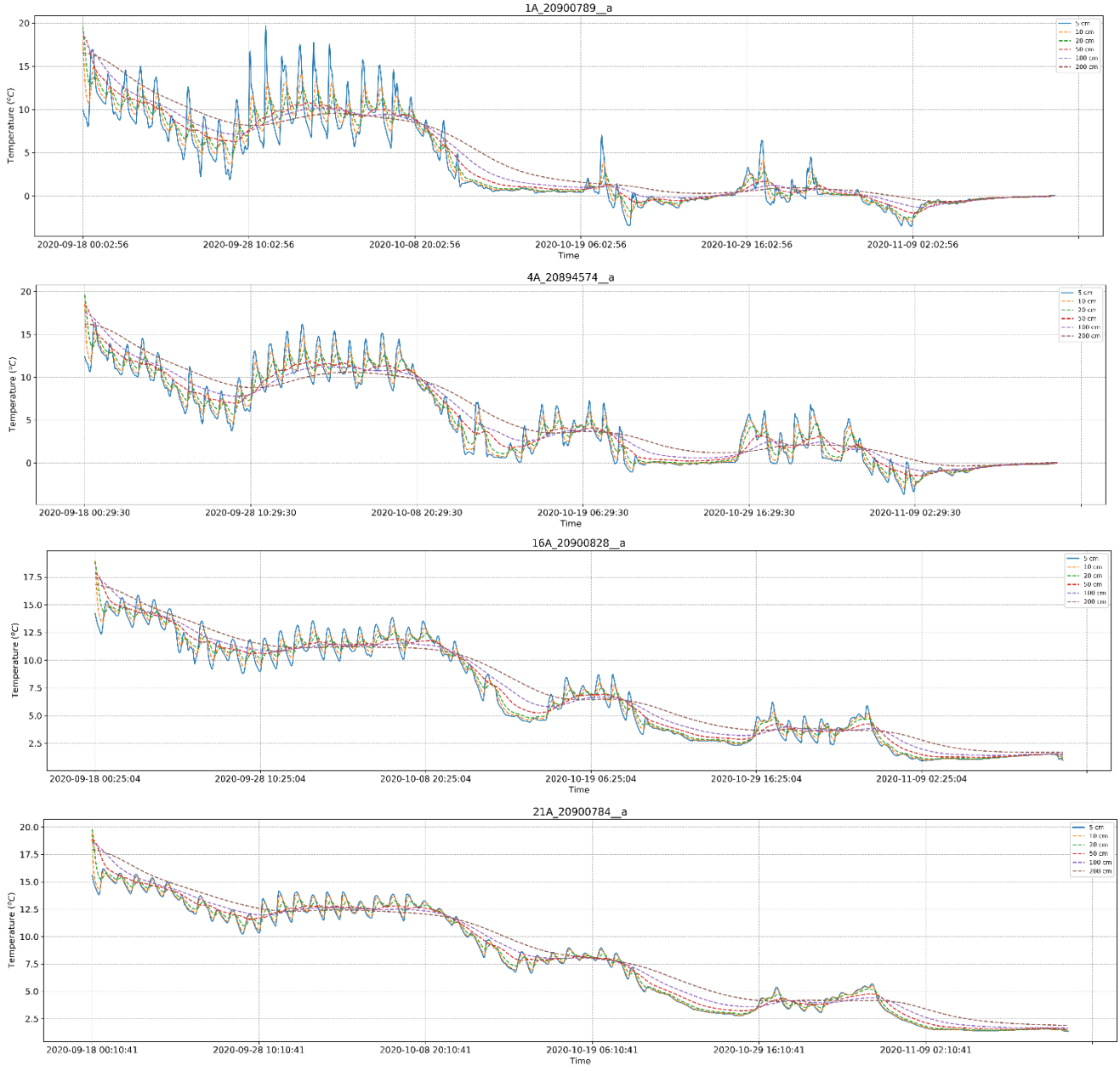

Figure 5. Samples of calculated thermal variation of 2 months period from September-18, 2020 at selected sites (1A; 4A; 16A; 21A).

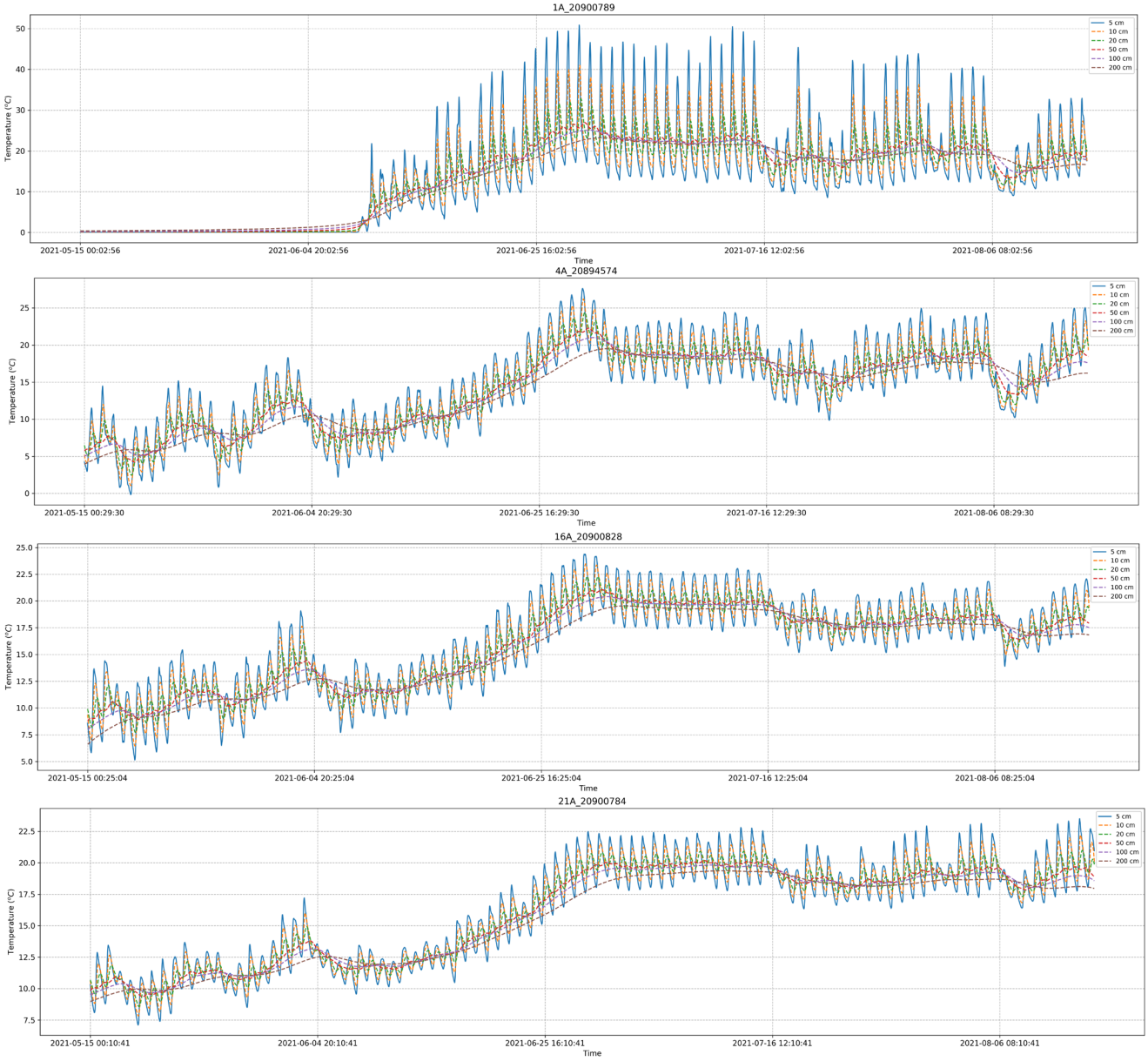

Figure 6. Samples of calculated thermal variation of 3 months period from May-15, 2021 at selected sites (1A; 4A; 16A; 21A).

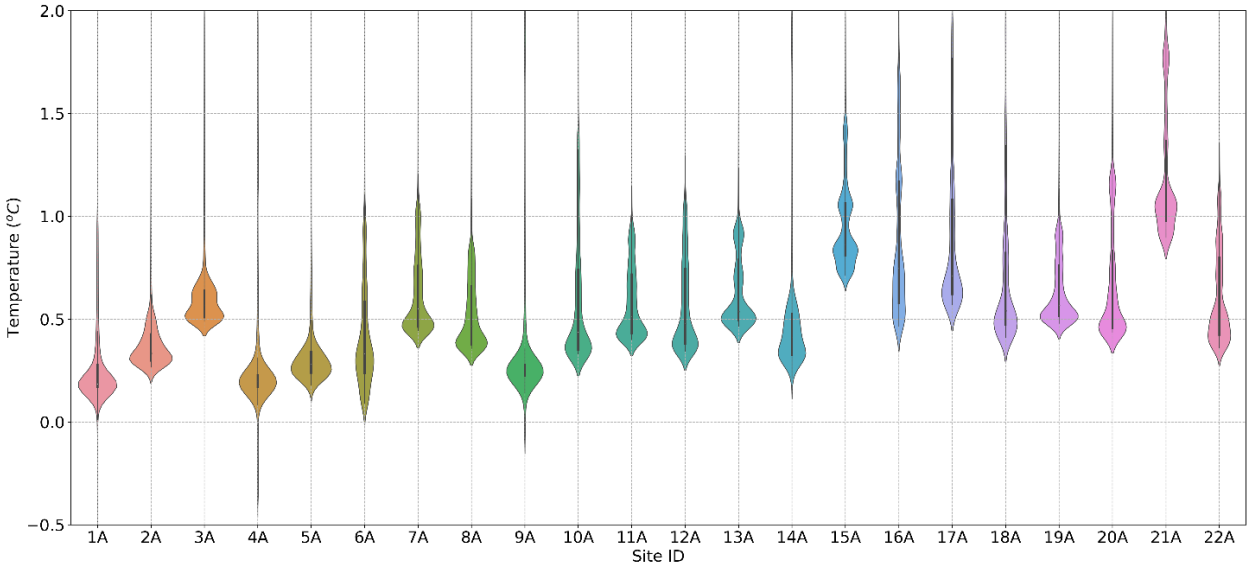

Figure 7. Plots showing predicted thermal statistics at 2.0 meters depth for all of sites in selected winter period.

Figure 8 shows four thermal anomalous indexes for identifying the potential location of high thermal flux. The four component indexes are standardized relative difference with gradient components in positive and negative directions $G_p = \frac{1}{n}\sum_{i=1}^{n}(T_i - T_{i-1})$; temperature difference between the peak and minimum temperature at 2.0 meter depth, $G_m = max(T_2) - min(T_2)$; and average temperature during winter (mid-November to March), $G_w = mean(T_2)$. Figure 9 shows the combined index normalized weighted summary with four indexes in Figure 8, we can see that there is a high relative difference of potential enhanced thermal flux surround sites 16A and 21A along Meager Creek.

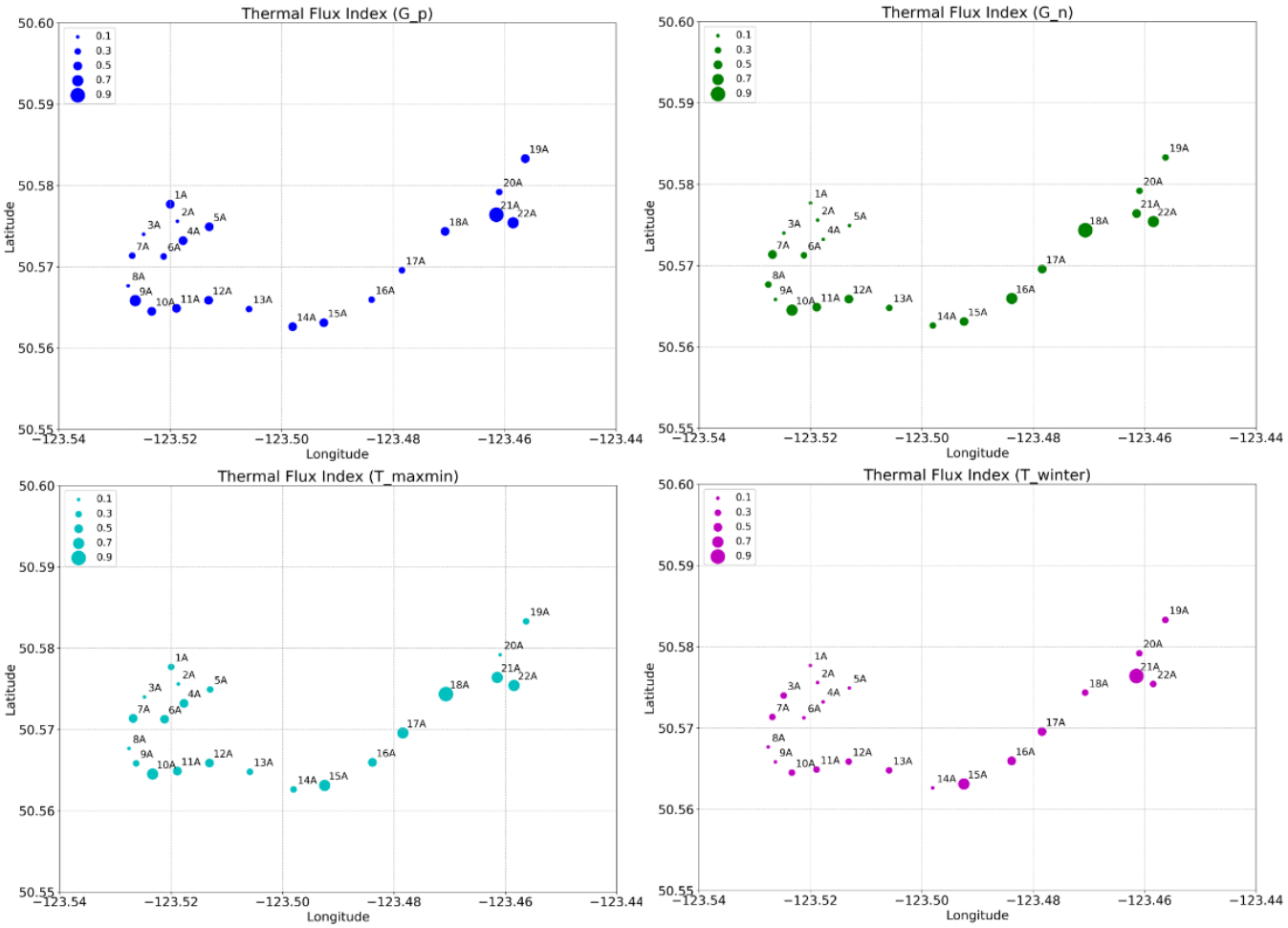

Figure 8. Calculated component indexes based on predicted thermal variation during summer and winter periods, (G_p means the positive gradient; G_n means the negative gradient; T_maxmin is the temperature difference during summer period; T_winter is the average temperature during the selected winter period), (The size of dots means the relative difference value of high thermal anomaly).

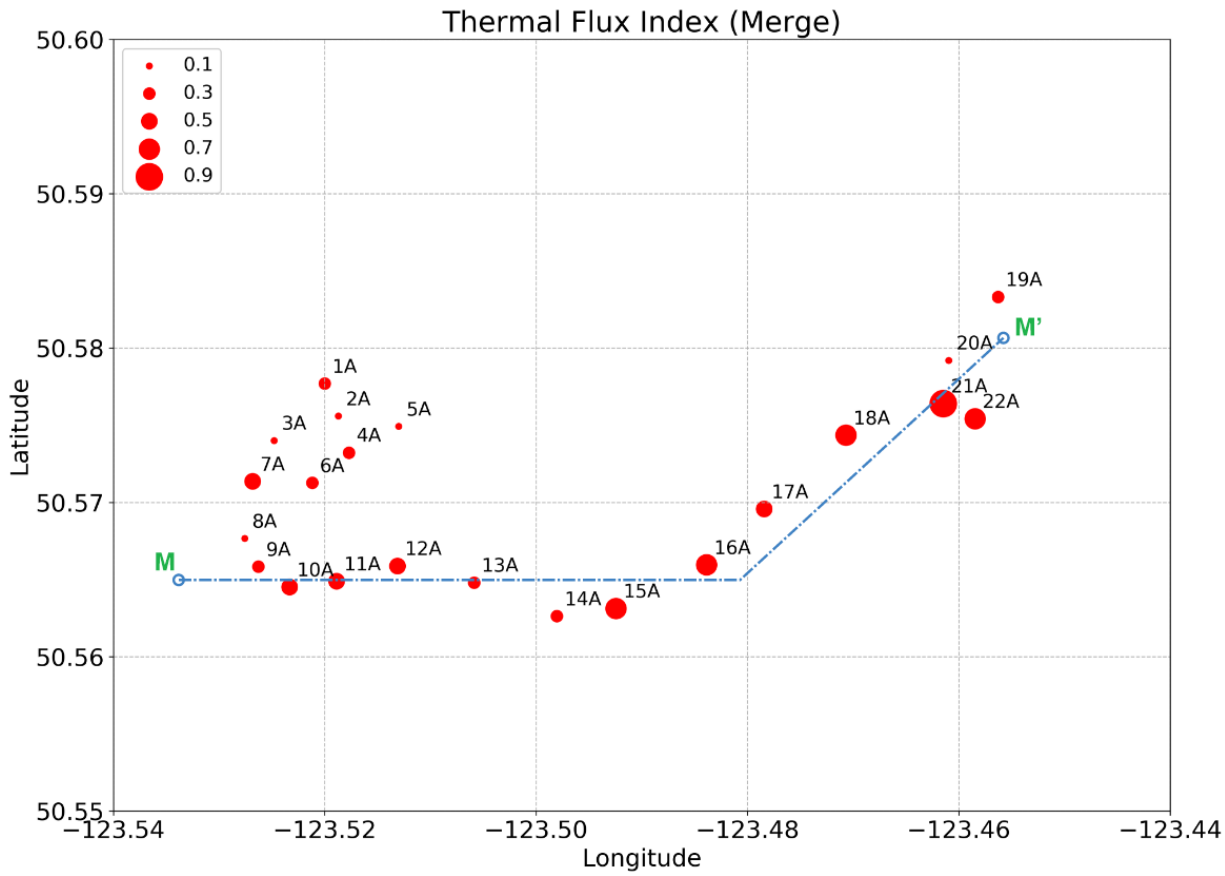

Figure 9. Relative difference distribution with concatenating four indexes in Figure 8, line M-M' is a schematic section.

5. Discussion and conclusions

5.1 Discussion

The collected data during summer time shows the high effect of daily solar thermal flux. Because of this effect, the calculated temperature of the near subsurface are not independent enough to reflect the effect of the upwarding geothermal source. In this study, we used the same apparent conductivity for all of probe sites, which might affect the predicted result. The thermal conductivity measurement of core samples would be also necessary for integrated comparison.

The simulation method with temperature variation in time series can produce a thermal variation trend, but the single temperature probe at each site in Mount Meager area can not remove the effect of solar thermal radiation and compute the geothermal flux value. With current data sets, we can only calculate the relative difference to show anomalous distribution of deep geothermal heat flux based on the relative difference indexes. During the snow covered period, recorded temperature is not accurate to reflect the seasonal variation because the thermal conductivity of snow is much smaller than surface rock or soil.

Based on previous studies (Fairbank, 1978, 1979; Lewis, 1978), we updated a profile (Fig. 10) that shows a selected vertical view in study area (see section M-M' in Fig. 9). Figure 10a shows the temperature logging profiles from different boreholes along the profile. We can see our calculated high relative difference points (16A, 21A) is consistent with nearby borehole temperature logs (M1-74D and 301-2) (Lewis, 1978), which show higher average temperature in shallow zone (<50 meters). This proved the shallow thermal gradient anomalous zone along Meager Creek, and the stability of statistic analysis with downward simulating temperature variation. More probe sites beside those wells will be useful to verify the anomalous zone in future study.

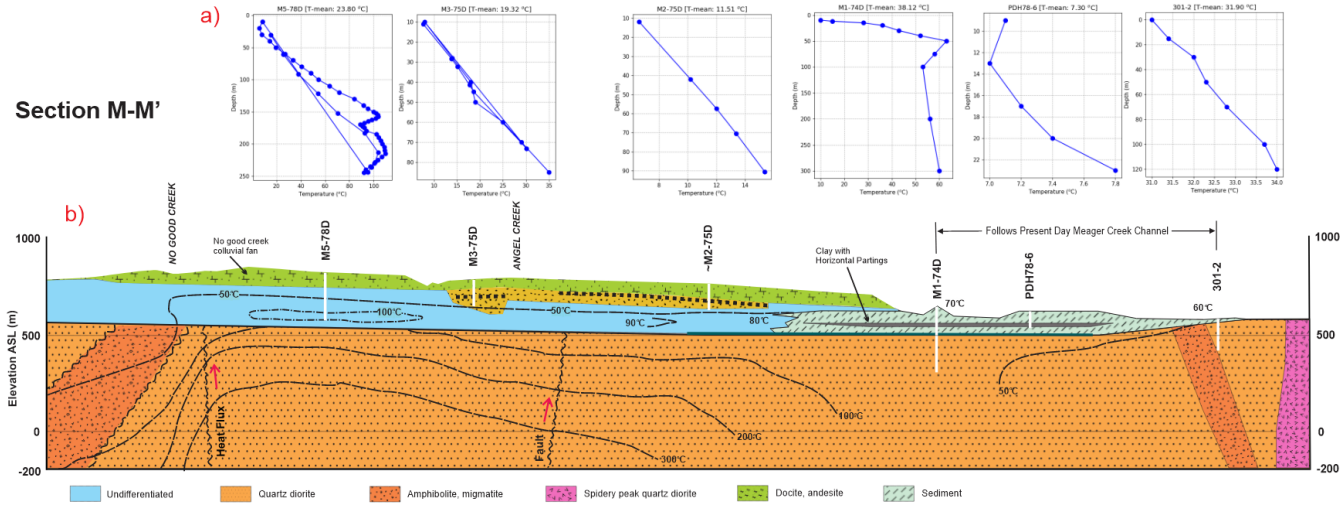

Figure 10. Vertical profile M-M' in study area, a) temperature log profiles of nearby wells along the section M-M'; b) section M-M' showing the reservoir temperature distribution and geologic settings (based on Fairbank, 1979).

Since the solar radiation is much larger than geothermal flux rate on near surface area, the depth of probes could be placed deeper in future surveys. For example, it works with measurement geometry of a few meters per set with 30 cm interval if can overcome difficult of drilling into hard rock (Fig. 11). The deeper temperature probe would be affected less by solar thermal flow and it would be easier to calculate the finite difference solution, which will improve the reliability of measuring and calculated flux from deep thermal source.

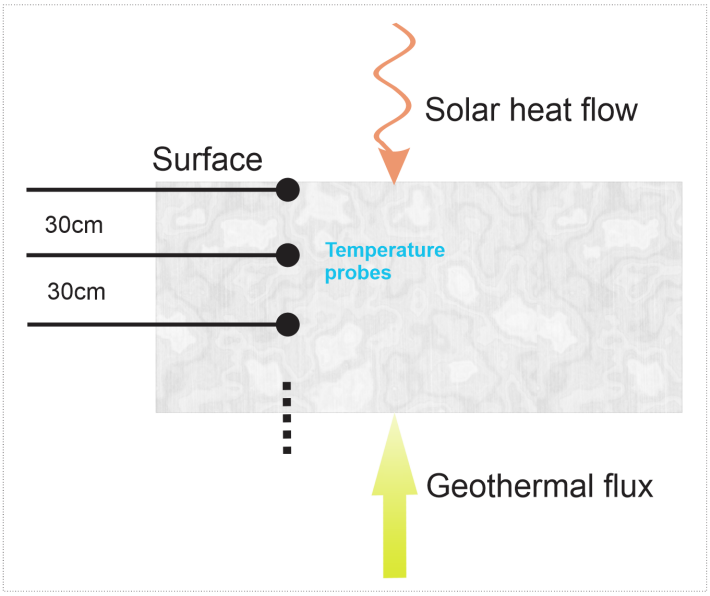

Figure 11. Schematic of heat flow and temperature measurement.

5.2 Conclusions

The pre-processing, analysis and interpretation framework of time-series temperature data is presented to extracted thermal flow anomaly with an inversion workflow and code with python language. This study is a first test of the potential of the algorithm in identifying the shallow thermal anomaly successfully. It can provide supporting information/evidence for regional surface thermal distribution, which is helpful for the geothermal resource assessment and exploration. Although a single-level shallow temperature is only measured, the interpreted results in Mount Meager area and comparing with previous study still help us identify a possible high thermal flux anomalous zone by fluid convection along the Meager Creek. Also, note that this methodology is generalizable to use for data analysis of multi-depths measurement. Integrated interpretation with other geoscience data will narrow the uncertainty and produce more accurate model results.

Acknowledgements

Thanks for the funding support of the Geoscience BC and Natural Resource Canada. The authors are grateful to research scientist Dr. Makram Hedhli at the Geological Survey of Canada for providing a comprehensive review and feedbacks of this study. We would also like to thank the students at Simon Frasor University helping deploy the temperature loggers in 2020 field season. Special thanks to Dr. Sonya Dehler and Dr. Edward Little for supporting and leading the GSC-Calgary's geothermal project. This represents an output from Geoscience for New Energy Supply.

Competing interests

All of the authors declare that there are not competing interests associated with the study.

References

[1] An, K., Wang, W., Zhao, Y., Huang, W., Chen, L., Zhang, Z., Wang, Q., and Li, W., 2016. Estimation from soil temperature of soil thermal diffusivity and heat flux in sub-surface layers, Boundary Layer Meteorol., 158(3), 473–488, doi:10.1007/s10546-015-0096-7.

[2] Assouline, D., Mohajeri, N., Gudmundsson, A. & Scartezzini, J. 2019, "A machine learning approach for mapping the very shallow theoretical geothermal potential", Geothermal energy (Heidelberg), vol. 7, no. 1, pp. 1-50.

[3] Bennett, W.B., Wang, J., and Bras, R.L., 2008. Estimation of global ground heat flux, J. Hydrometeor., 9(4), 744–759, doi:10.1175/2008JHM940.1.

[4] B.C. Hydro, 1983. Meager Creek Geothermal Project, Summary report for 1982-83. Meager Creek Project Staff, Vancouver, July 1983. 36 pp. plus figures.

[5] Campbell, G.S. 1985. Soil physics with basic transport models for soil-plant systems, Elsevier, New York; Amsterdam.

[6] Erkan, K., Blackwell, D.D., Leidig, M., 2005. Crustal thermal regime at the geysers/clear lake area, California. In: Processdings of the World Geothermal Congress, Antalya, Turkey, April 24-29, 9pp.

[7] Fairbank B.D., Canada. Energy, Mines and Resources Canada, B.C. Hydro, Nevin Sadlier-Brown Goodbrand Ltd. Report on 1978 Field Work Meager Creek Geothermal Area Upper Lillooet River, British Columbia. Vancouver, B.C: Nevin Sadlier-Brown Goodbrand Ltd; 1979.

[8] Fairbank, B.D., Reader, J. F., Sadlier-Brown, T. L., B.C. Hydro, & Nevin Sadlier-Brown Goodbrand Ltd. (1980). Report on 1979 drilling and exploration program meager creek geothermal area: Upper lillooet river, british columbia. Nevin Sadlier-Brown Goodbrand Ltd.

[9] Fourier J.B.J. 1822. Théorie analytique de la chaleur. Paris: Chez Firmin Didot, Père et Fils.

[10] Fuchs, S., Balling, N., Förster, A., 2015. Calculation of thermal conductivity, thermal diffusivity and specific heat capacity of sedimentary rocks using petrophysical well logs, Geophysical Journal International, Volume 203, Issue 3, December 2015, Pages 1977–2000, https://doi.org/10.1093/gji/ggv403.

[11] Gao, Z., Horton, R., and Liu, H.P., 2010. Impact of wave phase difference between soil surface heat flux and soil surface temperature on soil surface energy balance closure. Journal of Geophysical Research: Atmospheres, vol. 115, no. D16, pp.

[12] Gao, Z., Russell, E.S., Missik, J.E.C., Huang, M., Chen, X., Strickland, C.E., Clayton, R., Arntzen, E., Ma, Y., Liu, H. & Pacific Northwest National Lab. (PNNL), Richland, WA (United States), 2017. A novel approach to evaluate soil heat flux calculation: An analytical review of nine methods: Soil Heat Flux Calculation. Journal of geophysical research. Atmospheres, vol. 122, no. 13, pp. 6934-6949.

[13] GeothermEx, Inc. (1995). Daily geological reports for Pacific Geopower, well MC-5.

[14] GeothermEx, Inc., 2004. Report on the south Meager geothermal resource British Columbia, Canada.

[15] Grasby S.E. et al., 2012. Geothermal Energy Resource Potential of Canada. Open File, Vol 6914. Ottawa: Geological Survey of Canada, pp. 301.

[16] Grasby S.E. et al., 2020. Garibaldi Geothermal Energy Project Mount Meager 2019 - Field Report, Geoscience BC Report 2020-09, pp. 153.

[17] Gupta, H., and Roy, S., 2007. Geothermal Energy. 1st Edition - ISBN: 9780444528759, 9780080465647.

[18] Guthrie, R.H., Friele, P., Allstadt, K., Roberts, N., Evans, S.G., Delaney, K.B., Roche, D., Clague, J.J. & Jakob, M. 2012, "The 6 August 2010 Mount Meager rock slide-debris flow, Coast Mountains, British Columbia; characteristics, dynamics, and implications for hazard and risk assessment", Natural hazards and earth system sciences, vol. 12, no. 5, pp. 1277-1294.

[19] Hiraiwa, Y. and Kasubuchi, T., 2000. Temperature dependence of thermal conductivity of soil over a wide range of temperature (5-75℃). European Journal of Soil Science. vol. 51(2): 211-218.

[20] Horton, R., Wierenga, P.J., and Nielsen, D.R., 1983. Evaluation of methods for determining the apparent thermal diffusivity of soil near the surface. Soil Sci. Soc. Am. J. 47:25–32.

[21] Hurley, S. and Wiltshire, R.J., 1993, "Computing thermal diffusivity from soil temperature measurements", Computers & geosciences, vol. 19, no. 3, pp. 475-477.

[22] Jessop, A., 2008, Review of National Geothermal Energy Program, Phase 2 – geothermal potential of the Cordillera; Geo-logical Survey of Canada, Open File 5906, 86 p., https://doi.org/10.4095/225917.

[23] Lewis, T.J. and Souther, J.G., 1978, Meager Mountain, B.C. a possible geothermal energy resource. Energy Resource. Earth Physics Branch, Geothermal Series no. 9, 26 p. doi:10.4095/8433.

[24] Lu, Y., Lu, S., Horton, R., and Ren, T., 2014. An empirical model for estimating soil thermal conductivity from texture, water content, and bulk density, Soil Sci. Soc. Am. J., 78(6), 1859–1868, doi:10.2136/sssaj2014.05.0218.

[25] Read, P.B., 1979. Geology, Meager Creek Geothermal Area, British Columbia. Geological Society of Canada Open File Report 603, 1:20,000 scale map, legend and descriptive notes.

[26] Rybach, L., 1989. Heat flow techniques in geothermal exploration, First break, vol. 7, no. 1, pp. 9-16.

[27] Sauer, T.J., Ochsner, T.E., Horton, R., 2007. Soil Heat Flux Plates, Agronomy Publications. 375. https://lib.dr.iastate.edu/agron_pubs/375.

[28] Selker, J., Dani, O., 2019. Soil Hydrology and Biophysics. DOI:10.5399/osu/1142.

[29] Sestini, G., 1970. Heat flow measurement in non-homogeneous terrains; its application to geothermal areas. Geothermics, Vol 2(1), 424-436.

[30] Sharratt, B.S., Campbell, G.S., and Glenn, D.M., 1992. Soil heat flux estimation based on the finite-difference form of the transient heat flow equation. Agricultural and forest meteorology, vol. 61, no. 1, pp. 95-111.

[31] Vrugt, J.A., Gupta, H.V., Bastidas, L.A., Bouten, W. and Sorooshian, S., 2003. Effective and efficient algorithm for multiobjective optimization of hydrologic models, Water resources research, vol. 39, no. 8, pp. 1214-n/a.

[32] Zhdanov, M.S., 2002. Geophysical inverse theory and regularization problems. Elsevier Science, p.633.